Geophysical imaging of watershed subsurface patterns and prediction of soil texture and water holding capacity

H. Abdu,[1] D. A. Robinson,[2] M. Seyfried,[3] and S. B. Jones[4]

Received 28 March 2008; revised 17 August 2008; accepted 10 October 2008; published 23 December 2008.

[1] The spatial distribution of subsurface soil textural properties across the landscape is an important control on the hydrological and ecological function of a watershed. Traditional methods of mapping soils involving subjective assignment of soil boundaries are inadequate for studies requiring a quantitative assessment of the landscape and its subsurface connectivity and storage capacity. Geophysical methods such as electromagnetic induction (EMI) provide the possibility of obtaining high-resolution images across a landscape to identify subtle changes in subsurface soil patterns. In this work we show how EMI can be used to image the subsurface of a ~38 ha watershed. We present an imaging approach using kriging to interpolate and sequential Gaussian simulation to estimate the uncertainty in the maps. We also explore the idea of difference EC_a mapping to try to exploit changes in soil moisture to identify more hydrologically active locations. In addition, we use a digital elevation model to identify flow paths and compare these with the EC_a measurement as a function of distance. Finally, we perform a more traditional calibration of EC_a with clay percentage across the watershed and determine soil water holding capacity (SWHC). The values of SWHC range from 0.07 to 0.22 m^3 m^{-3} across the watershed, which contrast with the uniform value of 0.13 derived from the traditional soil survey maps. Additional work is needed to appropriately interpret and incorporate EMI data into hydrological studies; however, we argue that there is considerable merit in identifying subsurface soil patterns from these geophysical images.

Citation: Abdu, H., D. A. Robinson, M. Seyfried, and S. B. Jones (2008), Geophysical imaging of watershed subsurface patterns and prediction of soil texture and water holding capacity, *Water Resour. Res.*, *44*, W00D18, doi:10.1029/2008WR007043.

1. Introduction

[2] Hydrological research is at somewhat of an impasse with many advanced models relying on multiparameter calibration data. Limitations in the availability of relevant, spatially exhaustive measurements, hinders the advance of our hydrological understanding and description of watershed-scale processes. As a result many hydrologists are reflecting on the approaches used and trying to develop alternative ways that focus on the diagnosis of underlying patterns e.g., soils or vegetation [*McDonnell et al.*, 2007]. This dominant processes concept [*Sivakumar*, 2004] aims to identify fundamental patterns and controls on the hydrological processes operating in a watershed. It seeks to develop new modeling approaches to describe hydrological response [*McDonnell et al.*, 2007]. A major constraint to advancing the science is a lack of quantitative spatial data, identifying subsurface watershed soil patterns that can be used to constrain, test, or even conceptualize models and their frameworks at the watershed scale. In the same way that many hydrological modelers are exploring new approaches, so many scientists with an emphasis on measurement methods are exploring new technologies that can provide quantitative data of value to the hydrological sciences. Exciting new technologies include the use of distributed temperature sensing [*Selker et al.*, 2006], lidar surface mapping [*Lane and Chandler*, 2003], and lidar vapor mapping [*Cooper et al.*, 2000]. In addition, there is renewed interest in geophysical methods, through the emerging discipline of hydrogeophysics [*Rubin and Hubbard*, 2005; *Robinson et al.*, 2008b].

[3] Hydrogeophysics provides a useful tool for obtaining spatial data, with regard to earth properties, that are related to important hydrological parameters, and may be used to constrain hydrological modeling efforts. However, issues such as nonuniqueness of the signal response, scale of measurement and uncertainty are topics that need ongoing research [*Rubin and Hubbard*, 2005]. Examples of recent applications of geophysics for the very near surface include: exploiting magnetic properties to identify fault networks in sedimentary basins that will impact surface and groundwater flow [*Grauch and Millegan*, 1998]; the use of delay

[1]Department of Biological and Irrigation Engineering, Utah State University, Logan, Utah, USA.
[2]Department of Food Production, University of the West Indies, St. Augustine, Trinidad and Tobago.
[3]Northwest Watershed Research Center, ARS, USDA, Boise, Idaho, USA.
[4]Department of Plants, Soils and Climate, Utah State University, Logan, Utah, USA.

Copyright 2008 by the American Geophysical Union.
0043-1397/08/2008WR007043$09.00

time response of high-frequency electromagnetic (EM) waves to image changes in water table elevation [*Hyndman and Tronicke*, 2005]; exploiting the electrical resistivity properties of the unsaturated zone to monitor snowmelt and seasonal changes in soil moisture [*Daniels et al.*, 2005]; and using electrical properties, such as EM wave propagation time, to infer water content [*Ferré et al.*, 2005; *Huisman et al.*, 2003; *Robinson et al.*, 2008c], on the assumption that the propagation time is controlled by the dielectric properties of the porous media, which are in turn controlled by the vadose zone water content.

[4] Electromagnetic induction is a technique, originally developed for the oil industry and well logging, which has been exploited ~25 years in soils research to identify soil salinity [*Hendrickx and Kachanoski*, 2002; *Rhoades et al.*, 1999]. However, it is only in the more recent past that hydrologists have begun to consider its utility [*Kachanoski and de Jong*, 1988; *Sheets and Hendrickx*, 1995; *Sherlock and McDonnell*, 2003]. The application of electromagnetic induction (EMI) to hydrology has been somewhat limited, this most likely reflects the fact that measurements are easily made but less easily interpreted. A firm understanding of soil properties affecting electromagnetic field behavior is helpful in understanding when EMI can be applied, as it is not suitable for all circumstances. Like all geophysical methods, EMI exploits contrasts in soil geophysical response, in this case electrical, to estimate soil textural [*Doolittle et al.*, 1994; *Triantafilis et al.*, 2001; *Triantafilis and Lesch*, 2005] and hydrologic patterns [*Sherlock and McDonnell*, 2003]. Research has shown that the method can be used to estimate water content in soils [*Sheets and Hendrickx*, 1995], with the caveat that this is under circumstances where the differences in water content lead to measurable differences in soil electrical properties; this is unlikely to be the case in organic soil for instance.

[5] The traditional interpretation of EMI measurements is to try to produce calibrated maps of soil salinity or texture, and several procedures have been described [*Lesch et al.*, 1995a, 1995b]. Field-scale studies are beginning to explore alternative methods of interpreting the data, and recognize the important contribution that EMI can make to observing soil spatial variability and the identification of field-scale heterogeneities [*Corwin and Lesch*, 2005]. *Sherlock and McDonnell* [2003] applied this approach to hillslope studies and argued for the use of "soft data" in helping to interpret subsurface patterns.

[6] The aim of this research was to present and test an EMI mapping procedure for an entire watershed in order to delineate boundaries and spatial patterns in the subsurface as part of a broader ecohydrological study that focused on the difference between meadow grass and shrub plant communities. Further more, to compare this with Natural Resources Conservation Service (NRCS) soil survey maps of the watershed. The EMI mapping provides an opportunity to compare the quantitative subsurface geophysical image with the more qualitative soil survey interpretation on the basis of landscape and vegetation patterns. Difference mapping, wet and dry, is used to identify areas associated with "change" which might be interpreted in light of hydrological processes. In addition we create a texture map of the watershed based on the EMI response surface and soil sampling. Values of soil water holding capacity are interpreted from the map and compared with the traditional soil survey data.

2. Materials and Methods

2.1. Study Area

[7] The Reynolds Mountain East (RME, 43°04′ N and 116°45′ W) study area (Figure 1) encompassing ~38 ha is located on the southeastern tip of the larger 239 km^2 USDA Reynolds Creek Experimental Watershed in the Owyhee Mountains near Boise, Idaho, United States. The RME study area is monitored at five meteorological measurement stations, a snow course, soil temperature and soil moisture monitoring locations, precipitation stations, and a weir [*Slaughter et al.*, 2001; D. Marks et al., Long-term snow, climate and streamflow trends from the Reynolds Creek Experimental Watershed, Owyhee Mountains, Idaho, USA, submitted to *Water Resources Research*, 2008].

[8] The RME, a small perennial headwater catchment, ranges in elevation from 2010 m to 2140 m and is typical of a semiarid rangeland ecosystem with some steep slopes (up to 40%) and some shallow weakly developed soils [*Seyfried et al.*, 2001]. The soil survey map identifies the central woody area, and the northwestern part of the catchment, as the Parkay-Dehana (fine-loamy, mixed, superactive Pachic Argicryolls) association and the rest of the watershed as the Parkay-Bergar (loamy-skeletal, mixed, superactive Pachic Argicryolls) complex (Figure 1). The parent material of the soils comprises basalt and latite, and rocky outcroppings can be seen close to the ridges. The soil texture ranges from fine loam to clay and the clay percentage increases in proportion with depth toward fractured bedrock; the soil depth exceeds 3 m under some of the woodland communities [*Grant et al.*, 2004]. The average annual precipitation for RME is about 900 mm and most of it is received in the winter months as snow between November and April. Snowfall which accounts for 75% of the precipitation is affected by wind drifts which contribute to the unevenly distributed infiltration of water into the soil [*Marks et al.*, 2001].

[9] The vegetation at RME is typical of higher elevations and consists of forest and alpine communities. Big sagebrush (*Artemesia tridentata*) and grassland communities dominate most of the catchment, with a mixed dense forest in the middle consisting of Douglas fir (*Pseudotsugua menziesii*) and quaking aspen (*Populus Tremuloides*). There are patches of snowbrush (*Ceanothus Velutinus*) and willows (*Salix sp.*) line the edges of the riparian zone [*Grant et al.*, 2004; *Robinson et al.*, 2008a].

2.2. Mapping

[10] Apparent electrical conductivity (EC_a) is a proxy for subsurface physical properties and provides a measure of charge mobility due to the application of an electric field. It is defined as the ratio between current density (J, A m^{-2}) and electrical field (E, V m^{-1}) according to Ohm's law [*Paul*, 2004], with a unit of millisiemens per meter (mS m^{-1}). An EMI system transmits a low-frequency electromagnetic field into the subsurface without the need to establish contact with the ground. The alternating magnetic field in the subsurface in turn induces secondary current loops in proportion to the subsurface electrical conductivity. These

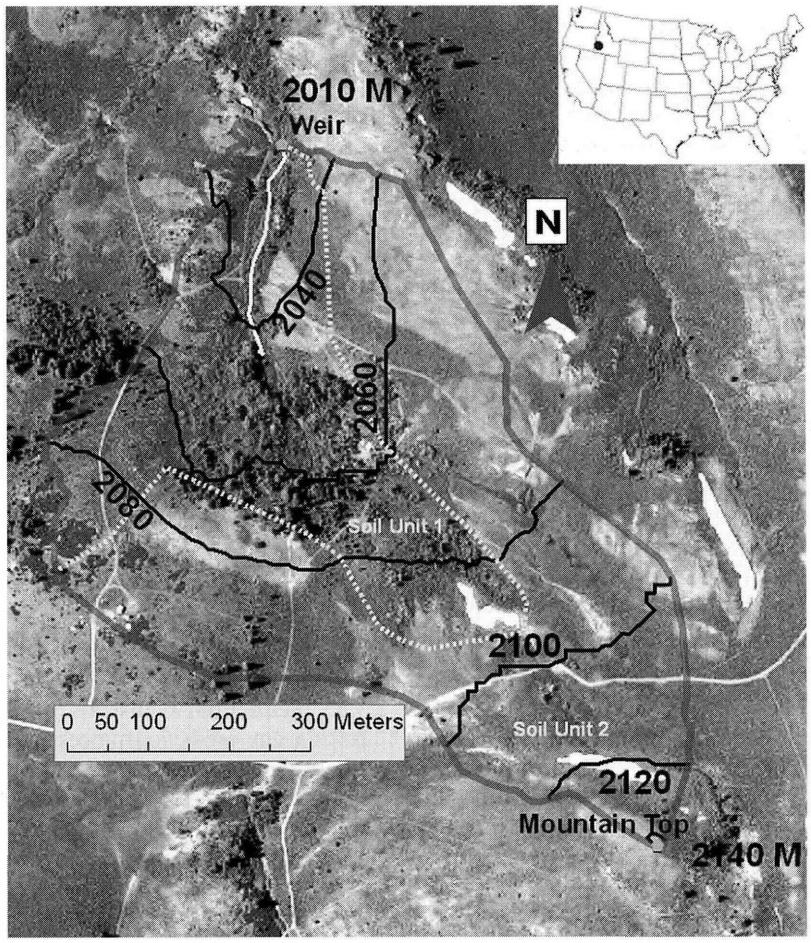

Figure 1. Air photo of the Reynolds Mountain East (RME, 43°04′N, 116°45′W) subwatershed boundary (red line), with contour lines in meters (black line), perennial stream (white line), and soil series delineation (dotted yellow line) from NRCS Soil Survey with soil unit 1 being classified as the Parkay-Dehana association and soil unit 2 as the Parkay-Bergar complex. See color version of this figure in the HTML.

create secondary magnetic field loops and the instrument measures the superposition of the combined primary and secondary fields [*McNeill*, 1980; *Abdu et al.*, 2007]. This noninvasive technique is appropriate for field-scale measurement because of its rapid response, ease of integration into mobile vehicular measuring platforms and nondestructive/noncontact requirements.

[11] Georeferenced EC_a measurements were taken noninvasively using the DUALEM-1S (Dualem, Milton, Ontario, Canada) ground conductivity instrument along with a Trimble (Trimble, Sunnyvale, California) ProXT GPS unit. The electromagnetic induction sensor provides a versatile and robust field instrument for determining bulk soil electrical conductivity. Electrical sensors are particularly suited to soil studies because the electrical conductivity of the earth is highly dependent on the electrical conductivity of the soil solution (EC_e), clay percentage and water content [*Friedman*, 2005]. The depth of exploration (DOE) for the vertical-vertical dipole setup (transmitter-receiver separation of 1 m) of the instrument is about 1.5 m [*McNeill*, 1980]. However, *Callegary et al.* [2007] have shown that in soils with conductivity that range up to 100 mS m^{-1} the DOE is reduced to less than 1 m. The EMI instrument was held ~40 cm above ground while traversing the watershed and this means that the effective DOE for the instrument was ~60 cm and the measurement volume was ~0.6 m^3. The georeferenced EC_a data was acquired using a handheld geographic information system (StarPal Inc., Fort Collins, Colorado) program inside an Allegro CX handheld field computer (Juniper Systems, Logan, Utah).

[12] The EMI instrument was turned on for 30 min for instrument stabilization before mapping the RME catchment on 12 July 2006 and 17 October 2007. The 2006 mapping was conducted a month after snowmelt and subsequent infiltration, leaving the ground saturated prior to evapotranspiration (ET) losses by vegetation. In contrast the 2007 mapping was done after the root zone soil moisture was depleted over the summer; some light rains in the weeks prior to mapping wetted the top part of the soil. Data from a soil moisture monitoring location in an aspen grove gives volumetric water content (θ_v) of 0.35 at the depth of 30 cm for both mapping days. At a deeper depth, the soil was much wetter for the 2006 mapping with θ_v of 0.40 and 0.59 for depths of 52 and 72 cm, respectively; while the 2007 mapping date had θ_v of 0.22 and 0.26 for depths of 52 and 72 cm, respectively. Simultaneous measurements of the soil EC_a at 30 and 52 cm were comparable between mapping events; 0.05 S m^{-1} at 30 cm for both mapping

events and 0.07 and 0.06 S m^{-1} at 52 cm for 2006 and 2007 mapping events, respectively. In the dense woody areas, the GPS signal was getting weak and we used the i.Trek M3 (i.Trek, Pasadena, California) GPS unit with the SiRF III chipset with its improved signal reception under the canopy. The EMI mapping process required a full day with EC_a data being collected every second. The EC_a data were then checked for continuity and anomalous values using a time series view of the data. Anomalous values (4% of the original data), which can be caused by buried metal fragments, wires, pipes, etc., were identified and removed from the data set as a quality control measure.

2.3. Geostatistics

2.3.1. Spatial Prediction

[13] Kriging relies on the underlying spatial structure of a measured variable in order to predict its value at unsampled locations [*Goovaerts*, 1999; *Webster and Oliver*, 2001]. Let $z(\mathbf{u}_\alpha)$, $\alpha = 1,2, \ldots n$ (with location vector $\mathbf{u}_\alpha$), being a realization of random variables (RV) $Z(\mathbf{u}_\alpha)$, describe the set of n EC_a values measured in the watershed. Most prediction methods, including kriging, average the weighted values of the adjacent sampled values, $z(\mathbf{u}_\alpha)$, in order to predict the variable, $z^*(\mathbf{u})$, at an unsampled point:

$$z^*(\mathbf{u}) = \sum_{\alpha=1}^{n} \lambda_\alpha z(\mathbf{u}_\alpha) \tag{1}$$

[14] The kriging estimator is given as the best linear unbiased estimator and thus kriging weights, λ_α, are determined by requiring unbiasedness and minimum estimation variance. The spatial dependence of the process, represented in the residuals of a generalized least squares regression equation, is solved when

$$\lambda_\alpha = C^{-1}c(\mathbf{u}) \tag{2}$$

where C is the matrix of covariances, $C(\mathbf{u}_\alpha, \mathbf{u})$, between all possible pairs of the n sample sites and $c(\mathbf{u})$ is a column vector of covariances between the prediction point and each of the n sample sites.

[15] In order to solve for λ_α we need to evaluate the matrix of covariances C, which can be done using a semivariogram function, written

$$\gamma(\mathrm{h}) = \frac{1}{2N(\mathrm{h})} \sum_{\alpha=1}^{N(\mathrm{h})} [z(\mathbf{u}_\alpha) - z(\mathbf{u}_\alpha + \mathrm{h})]^2 \tag{3}$$

where the function computes the average squared differences of the values of the random variable at a vector of data pairs $\mathbf{u}_\alpha$ and $\mathbf{u}_\alpha$+ h, where N(h) is the number of data pairs within a given class of distance. A parametric model is used to describe the experimental semivariogram to provide a continuous, positive and smooth description of the covariance matrix, C.

[16] Block kriging extends the above method from a point estimation of a spatially continuous variable to the average value over a small area or block [*Deutsch and Journel*, 1998]. This is useful when the support block of a physical measurement is beyond a point as in EMI measurements.

2.3.2. Data Transformation Using the Normal Score Procedure

[17] The prediction of a property of interest at unsampled areas using kriging requires the data to be normally distributed, since a normal distribution is completely defined by its mean and covariance function to establish its spatial distribution [*Webster and Oliver*, 2001]. The normal score transform is useful in normalizing many environmental variables that have nonuniform distributions or that may be positively skewed, providing a normal distribution [*Goovaerts*, 1997]. The normal score transform function is derived by matching the original skewed cumulative distribution function (cdf) to a standard normal cdf. Let a random function (RF) $\mathbf{Z}(\mathbf{u})$ consist of a set of usually dependent random variables (RV) $Z(\mathbf{u}_\alpha)$, $\alpha = 1,2, \ldots n$ for each location vector $\mathbf{u}_\alpha$ in the study area. Then the transform, $\varphi(.)$, that takes any RF $\mathbf{Z}(\mathbf{u})$ with cdf $F(z)$ to an RF $\mathbf{Y}(\mathbf{u})$ with a standard Gaussian cdf $G(y)$ is given as

$$\mathbf{Y}(\mathbf{u}) = \varphi(Z(\mathbf{u})) = G^{-1}[F(Z(\mathbf{u}))] \tag{4}$$

where $G^{-1}(.)$ is the inverse Gaussian cdf of the random function $\mathbf{Y}(\mathbf{u})$ [*Goovaerts*, 1997].

2.3.3. Sequential Gaussian Simulation

[18] In any prediction process, quantifying the uncertainty of the estimate is important to the end user. Kriging, which gives the minimum local error variance in the generalized least square sense, is affected by a smoothing of the local variance of the attribute being predicted. Even though the kriging variance quantifies the quality of a prediction, it is independent of the data values and assesses only the uncertainty of the data configuration, i.e., the spatial distribution of sampled data [*Deutsch and Journel*, 1998; *Goovaerts*, 1999].

[19] The spatial variability of the attribute (e.g., EC_a) being predicted can be better captured from the data using the sequential Gaussian simulation method (SGSIM) [*Goovaerts*, 1997]. Conditional simulation or stochastic imaging generates equally probable realizations of the property being studied in order to better quantify the uncertainty of the property at unsampled areas. Simulation focuses on honoring the data values while replicating the statistics of the data distribution and the variogram model [*Goovaerts*, 1999].

[20] In a kriging process, for each node a mean and variance is estimated thus the variable at the node can be represented as a Gaussian random variable. While kriging chooses the mean as an estimate of the node, SGSIM chooses the value of the node randomly from the Gaussian distribution.

[21] SGSIM can be implemented on each node of the prediction grid using the following algorithm [*Deutsch and Journel*, 1998].

[22] 1. We first define a random path that visits each node of the grid once. At each node $\mathbf{u}_\alpha$, a specified number of neighboring conditioning data including both original data and previously simulated grid node values are retained.

[23] 2. We then use kriging with a normal score variogram model to determine the parameters (mean and variance) of the conditional cdf of the RF $\mathbf{Z}(\mathbf{u})$ at location $\mathbf{u}_\alpha$.

[24] 3. A simulated value $z^{(l)}(\mathbf{u}_\alpha)$ is chosen randomly from the conditional cdf.

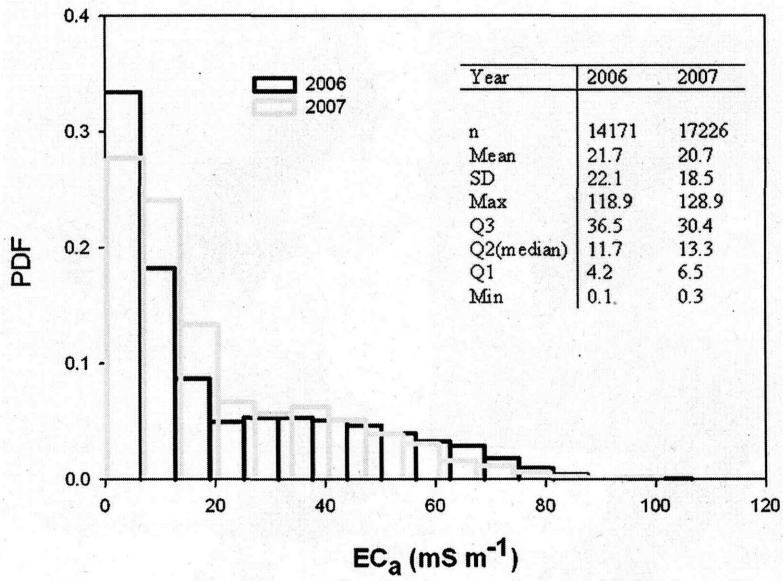

Year	2006	2007
n	14171	17226
Mean	21.7	20.7
SD	22.1	18.5
Max	118.9	128.9
Q3	36.5	30.4
Q2(median)	11.7	13.3
Q1	4.2	6.5
Min	0.1	0.3

Figure 2. Histogram and summary of the distribution statistics of EC_a for the 2006 and 2007 surveys. See color version of this figure in the HTML.

[25] 4. The simulated value $z^{(l)}(\mathbf{u}_\alpha)$ is added to the data set.

[26] 5. The above steps are repeated until all nodes are simulated.

2.4. Channel Network Extraction

[27] Techniques that extract channel networks from digital elevation models (DEM) have been used successfully to delineate stream networks [*Tarboton et al.*, 1991]. The DEM is first smoothed by locally filling spurious depressions to ensure that all pixels flow to a neighbor that will eventually drain to lower elevation. Flow directions are then evaluated for each pixel in order to calculate the number of upstream pixels that flow into each pixel. Those pixels that have accumulation areas exceeding the threshold of 15000 m^2 (150 pixels) were then delineated as part of a channel network.

2.5. Calibration Site Selection

[28] The spatial site selection algorithm in the ESAP software package [*Lesch et al.*, 2000] was used in order to pick out twenty calibration sites where soil was sampled for subsequent lab analysis. The selection algorithm that uses response surface methodology was developed by *Lesch et al.* [1995b] to predict field-scale soil salinity from EC_a survey data using multiple linear regression (MLR) models and a limited quantity of calibration samples. We adopted the site selection technique to predict field-scale clay percentage due to the high correlation between soil textural properties and EC_a in low-EC_e soils such as those found in the study site. The sample correlation between EC_a and clay percentage for the 2006 mapping were r = 0.93, 0.89 and 0.92 for 0–30 cm, 30–60 cm and 0–60 cm depth samples, respectively.

[29] The calibration sites are chosen such that they embody spatially the full surveyed region and that the corresponding EC_a data at the calibration sites allow efficient evaluation of the MLR parameters. The EC_a data was first centered and scaled by normalizing by the mean and standard deviation (i.e., mean of 0 and variance of 1) before the data was uncorrelated by applying a principal components analysis. The transformed EC_a data was then compared to a second-order central composite response surface design levels [*Box and Draper*, 1987]; the set of sites which are closest to the design levels and spatially cover the survey area adequately, were selected to be the calibration sites [*Lesch et al.*, 1995b].

[30] Soil physical characteristics were determined for the sampling locations down to 60 cm including, water content, texture, and EC_e. Particles larger than 2 mm were removed from the samples prior to textural analysis [*Natural Resources Conservation Service*, 1999]. Soil texture was determined using hydrometer analysis [*Gee and Or*, 2002]. These properties along with bulk density were input to Rosetta [*Schaap*, 1999], a pedotransfer function program that computes the van Genuchten soil hydraulic parameters including residual, θ_r, and saturated, θ_s, water contents. The soil water holding capacity was computed as $(\theta_s/2 - \theta_r)$ yielding soil water holding capacity in $cm^3\ cm^{-3}$. These values were then adjusted for the gravel content (averaging 20% by volume for the samples), estimating the in situ soil water holding capacity. Stepwise regression was then used to choose from the linear, quadratic, and interaction terms of the calibration sites' EC_a and spatial coordinates to select the MLR model variables. The most efficient model was that minimizing the prediction sum of square error residuals (PRESS) statistical criteria [*Lesch et al.*, 1995b].

3. Results and Discussion

3.1. Exploratory Data Analysis

[31] An exploratory univariate data analysis was performed on the georeferenced EC_a data that was collected for the two mapping dates. The data for the 2006 and 2007 data are comparable and have means that are very close; 21.7 and 20.7, respectively. The probability density function also shows the similarity between the two data sets collected more than a year apart (Figure 2). According to the distribution

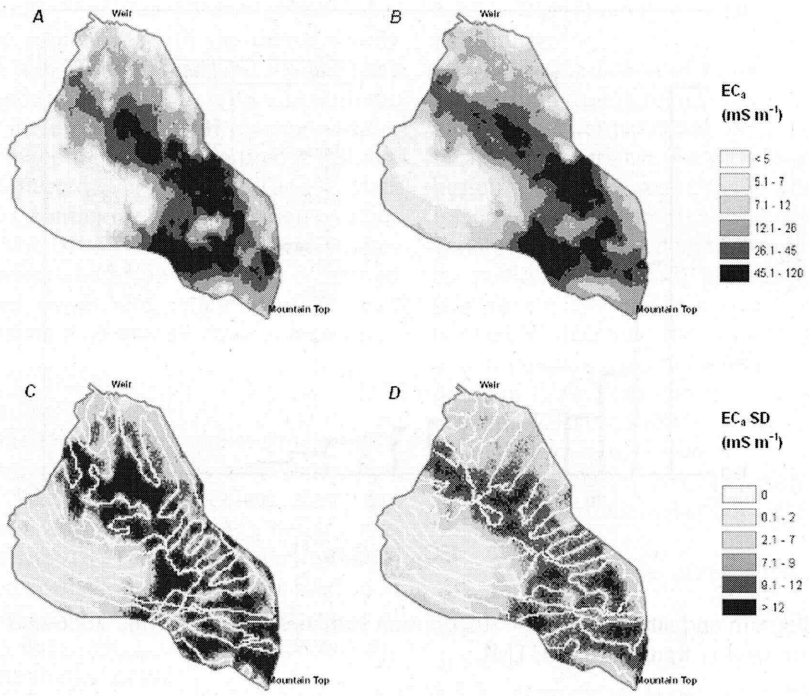

Figure 3. Sequential Gaussian simulation (SGSIM) maps aggregated from 50 realizations for (a) 2006 and (b) 2007 and (c and d) the respective standard deviation maps. See color version of this figure in the HTML.

statistics, the 2006 EC_a survey exhibits higher upper quartile values corresponding to the deep high water holding capacity soils; while the 2007 survey has a higher range of lower quartile values because of drier soils.

3.2. Spatial Prediction of EC_a

[32] We used semivariogram modeling to capture the spatial correlation of the EC_a survey data. An isotropic exponential model with a nugget of 0.02, range of 350 m and a sill of 1 (normal score transformed data) and a spherical model with a nugget of 0.05, range of 280 m and a sill of 1 were used to perform ordinary block kriging on a 5 × 5 m pixel for the 2006 and 2007 EC_a surveys, respectively. The longer range and smaller nugget for the moist soil from 2006 is consistent with the findings of *Western et al.* [1999], who observed the same pattern for measurements of volumetric water content across a small watershed. The kriged maps for the 2 mapping years, which are partitioned into 6 quantiles (Figures 3a and 3b), exhibit similar spatial patterns. Both maps show a low-EC_a area on the southwest corner of the watershed and the highest third of the EC_a values are located in the center, from the south of the watershed to the northwest.

[33] SGSIM was used to produce maps of prediction uncertainty for EC_a such as the standard deviation (SD) in Figures 3c and 3d by aggregating 50 realizations of the underlying random process. Since SGSIM honors the observed data, the survey routes stand out on the maps with SD values of zero. The low-conductivity area on the southwest corner of the watershed has a lower SD for both years (<7 mS m^{-1}). The standard deviation increases in the high-conductivity regions and especially in areas where the distance between survey points is the furthest. Overall, lower values of SD for the 2007 survey are observed and can be attributed to the better EC_a survey coverage of the watershed.

[34] The difference between "wet" and "dry" predicted EC_a maps can also be used to study the soil morphology of the catchment. It also helps to identify hydrologically active locations in a qualitative sense, i.e., locations where water may be accumulating or depleting. We subtracted the dry (2007) EC_a map from the wet (2006) map and examined the change in EC_a as a proxy for observing changes in water storage (Figure 4a). We interpret the areas with a large positive change to be associated with deep soils that have higher clay percentage and higher water holding capacity, those with little or no change as shallow often more stony soils, while those locations with a high negative change we interpret as soils with the possibility of some ion accumulation [*Friedman*, 2005]. The areas exhibiting the largest changes are consistent with the eastern side of the watershed. These areas are also locations where more vegetative growth is observed and may indicate water use by the trees and shrubs (Figure 4b).

3.3. EC_a and Channel Networks

[35] Using a 10 m DEM, those pixels which received contribution from an upper catchment area of 150 pixels (15,000 m^2) were designated as being part of a channel network (Figure 5a). This DEM derived network can be compared with the surface water channel plotted in Figure 1. The DEM network allows estimation of the expected location of subsurface flow paths according to the surface topography. We then looked at how the average EC_a of a 5 m buffer area varied as the buffer moved away from the channel network (Figure 5b). For the 2006 SGSIM map, we observe a constant decline in the average EC_a up to 50 m away from the channel network and subsequent leveling of

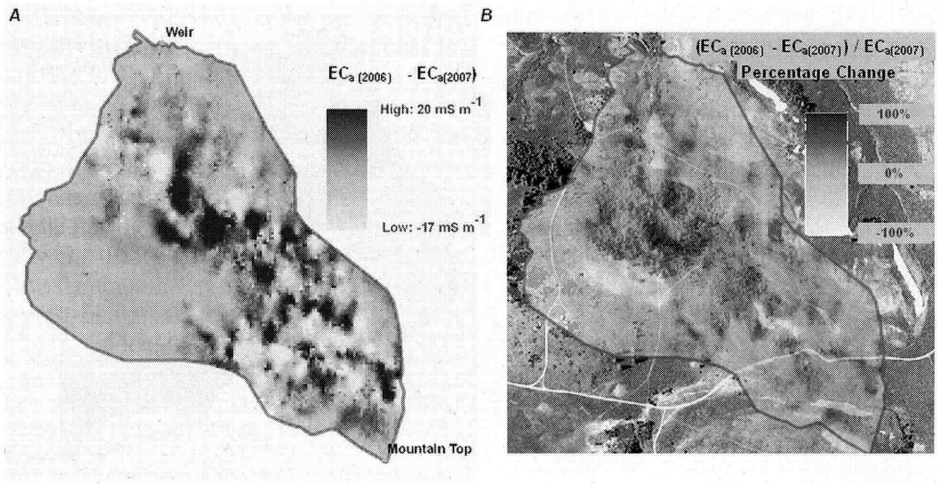

Figure 4. Maps of (a) 95th percentile difference in EC_a from 2006 to 2007 and (b) transparent overlay of the percentage difference in EC_a over an air photo of the watershed. See color version of this figure in the HTML.

the average EC_a for the next 100 m. This is in broad agreement with the concept of soil catena, from which we would expect the fine textured materials to accumulate in downslope positions in the landscape. Given the strong correlation between clay percentage and the EMI measurement, this is strong qualitative evidence that the EMI mapping is picking up the soil textural patterns of the watershed.

3.4. Clay Percentage Map

[36] A multiple linear regression (MLR) model was used to produce a clay percentage map for the top 0.6 m of the RME watershed (Figure 6a). Stepwise linear regression was applied to identify EC_a followed by latitude (Northing) as significant covariates to fit the MLR model. The model is written

$$\text{clay percentage} = 14.98 + 6.87\ y + 10.31\ z \qquad (5)$$

where y and z are the normalized latitude (northing) coordinate and the normal score transformed EC_a measurements, respectively.

[37] Using these variables as predictors, the proportion of variability in the data that is accounted for by the MLR model was given as $R^2 = 0.86$ and the RMSE of the model was 4.4%. The map was divided into six classes corresponding approximately to clay percentage boundaries on the USDA soil textural triangle indicating change in soil textural class. This map can be compared with the soil survey map showing the two soil series mapped for the site (Soil Survey Staff, Natural Resources Conservation Service, 2008, http://websoilsurvey.nrcs.usda.gov/). The soil survey map classifies both soils as clay loam with ~20% clay (http://websoilsurvey.nrcs.usda.gov/). Figure 6a indicates that the clay percentage is not uniform and varies from <10% to >36%. Hydrological modeling based on the soil survey data would treat the soils as uniform across the entire watershed, In

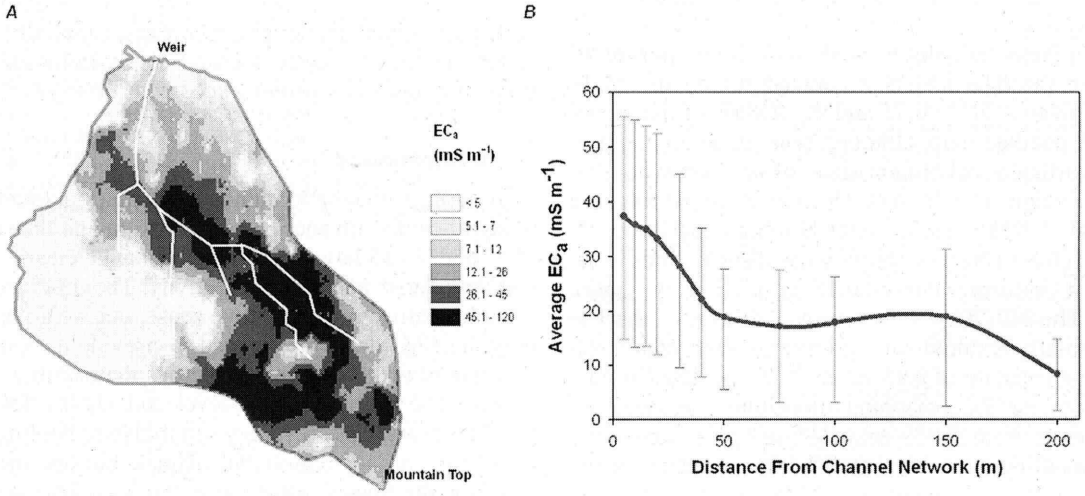

Figure 5. (a) Delineation of channel networks from a 10 m DEM with accumulation area threshold of 15,000 m^2 and (b) relationship between distance from channel and average EC_a for the 2006 SGSIM map. See color version of this figure in the HTML.

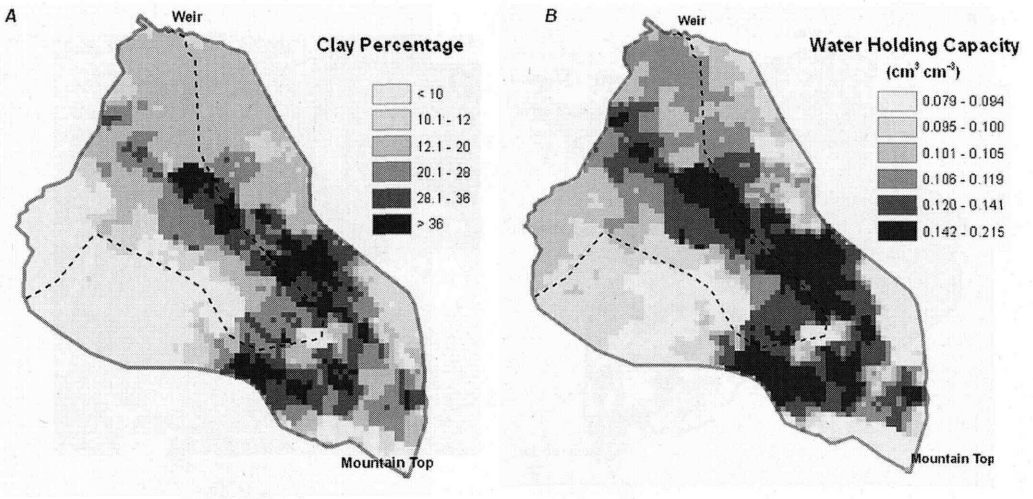

Figure 6. (a) Kriged clay percentage map and (b) water holding capacity map produced from the 2006 EC_a survey and the NRCS soil delineation line (dashed line). See color version of this figure in the HTML.

semiarid environments, where the available water is the limiting factor on biological processes, a texture map would be useful in estimating the amount of biologically available water [*Newman et al.*, 2006]. A spatially detailed texture map can demonstrate the role of soil texture in controlling plant distribution and vegetation structure by determining the distribution and duration of water storage [*Fernandez-Illescas et al.*, 2001; *Robinson et al.*, 2008a].

3.5. Soil Water Holding Capacity Map

[38] Following the procedure outlined in section 2.5, a soil water holding capacity map for the top 0.3 m of the RME watershed was generated. Stepwise linear regression was applied to identify EC_a followed by latitude (northing) as significant covariates to fit the MLR model. The model is written

$$\text{soil water holding capacity} = 0.110 + 0.021\ y + 0.021\ z \quad (6)$$

where y and z are the normalized latitude (northing) coordinate and the normal score transformed EC_a measurements, respectively.

[39] Using these variables as predictors, the proportion of variability in the data that is accounted for by the MLR model was given as $R^2 = 0.75$ and the RMSE of the model was 0.01. A detailed map, although nonunique and contingent upon particular calibration sites, of soil water holding capacity is obtained (Figure 6b). The map obtained from the conventional approach using water holding capacity available from Web Soil Survey (http://websoilsurvey.nrcs.usda.gov/) gave a uniform value of 0.13 m^3m^{-3} for the entire watershed. The NRCS soil survey map delineates the site into two similarly textured soils (Figure 1), each with a soil water holding capacity of 0.13 $m^3\ m^{-3}$. In the detailed map obtained from the EC_a mapping procedure, the range of SWHC extends from 0.079 to 0.215 $m^3\ m^{-3}$ across the watershed resulting in an integrated storage capacity for the top 0.3 m of the catchment of 12,900 m^3 compared to 14,800 m^3 using the generalized NRCS data. In this particular example the soils appear to have been mapped following the vegetation boundary (Figure 1), which in this case is an unsuitable boundary indicator as indicated by the geophysical EMI map (Figures 3a and 3b). Such spatially detailed storage maps can be useful in studying the discrepancy between measured hydrographs and model predictions, where average values used for soil moisture and soil hydraulic parameters can lead to large deviations [*Merz and Plate*, 1997]. Accounting for the spatial variability of infiltration properties is important in understanding runoff production [*Michaelides and Wilson*, 2007; *Woolhiser et al.*, 1996], and the role of organizational patterns of soil moisture on catchment runoff [*Merz and Plate*, 1997]. Such maps will be useful in understanding the effect of the spatial correlation of infiltration patterns in runoff pathways connectivity as well as modeled runoff uncertainty [*Michaelides and Wilson*, 2007].

[40] Soil mapping is no easy task, and clearly in this instance the geophysical method proves superior for this scale of watershed. However, for larger areas handheld geophysical mapping becomes infeasible, and soil survey maps remain the only current option. However, advances in airborne geophysical methods may provide the option of collecting spatial data over larger areas, especially with new techniques more clearly focused on hydrological applications of geophysics [*Robinson et al.*, 2008b].

4. Conclusions

[41] Electromagnetic induction mapping is demonstrated to significantly advance our ability to image the subsurface of a small (~38 ha) watershed. The image clearly identifies soil boundaries and soil connectivity. The observed patterns are informative in a qualitative sense, but we go on to show how the EMI data can be used to provide a more detailed estimate of watershed soil properties than simply using soil survey. The traditional low-level soil survey for the area provides a watershed average soil moisture holding capacity of 0.13 $m^3\ m^{-3}$, a reasonable estimate but one that lacks in showing the spatial patterns of the soil. The geophysical image captures the soil patterns and their connectivity and provides an area average SWHC of 0.11 $m^3\ m^{-3}$ with a range varying between 0.07 and 0.21 $m^3\ m^{-3}$. More over,

by differencing EMI maps observed during wet and dry periods we can identify hydrologically active locations. In addition, combining the EMI map with DEM derived flow paths gives insight into the spatial textural structure in relation to distance from a flow path. The data and its interpretation indicates the usefulness of geophysics in mapping small watersheds and opens a new opportunity to combine measurement and modeling approaches to better understand watershed-scale hydrological processes.

[42] **Acknowledgments.** We would like to thank Rosemary Knight at Stanford University for the support of the CUAHSI HMF Geophysics facility. This material is based upon work supported by the National Science Foundation under grants 03-26064 and 04-47287. This research was supported by a grant from the Inland Northwest Research Alliance (INRA) and by the Utah Agricultural Experiment Station, Utah State University, Logan, Utah, approved as journal paper 8013. Any opinions, findings, and conclusions or recommendations expressed in this material are those of the authors and do not necessarily reflect the views of the National Science Foundation. The use of firm, trade and brand names in this report is for identification purposes only and does not constitute endorsement by CUAHSI, NSF, the United States government, or the authors and their respective institutions.

References

Abdu, H., D. A. Robinson, and S. B. Jones (2007), Comparing bulk soil electrical conductivity determination using the DUALEM-1S and EM38-DD electromagnetic induction instruments, *Soil Sci. Soc. Am. J.*, *71*, 189–196.

Box, G. E. P., and N. R. Draper (1987), *Empirical Model-Building and Response Surfaces*, 700 pp., John Wiley, New York.

Callegary, J. B., T. P. A. Ferré, and R. W. Groom (2007), Vertical spatial sensitivity and exploration depth of low-induction-number electromagnetic-induction instruments, *Vadose Zone J.*, *6*, 158–167, doi:10.2136/vzj2006.0120.

Cooper, D. I., W. E. Eichinger, L. Hipps, J. Kao, J. Reisner, S. Smith, S. M. Schaeffer, and D. G. Williams (2000), Spatial and temporal properties of water vapor and flux over a riparian canopy, *Agric. For. Meteorol.*, *105*, 161–183, doi:10.1016/S0168-1923(00)00180-5.

Corwin, D. L., and S. M. Lesch (2005), Apparent soil electrical conductivity measurements in agriculture, *Comput. Electron. Agric.*, *46*, 11–43, doi:10.1016/j.compag.2004.10.005.

Daniels, J. J., B. Allred, A. Binley, D. LaBrecque, and D. Alumbaugh (2005), Hydrogeophysical case studies in the vadose zone, in *Hydrogeophysics*, edited by Y. Rubin and S. S. Hubbard, pp. 413–440, Springer, New York.

Deutsch, C. V., and A. G. Journel (1998), *GSLIB: Geostatistical Software Library and User's Guide*, 2nd ed., 369 pp., Oxford Univ. Press, New York.

Doolittle, J. A., K. A. Sudduth, N. R. Kitchen, and S. J. Indorante (1994), Estimating depths to claypans using electromagnetic induction methods, *J. Soil Water Conserv.*, *49*, 572–575.

Fernandez-Illescas, C. P., A. Porporato, F. Laio, and I. Rodriguez-Iturbe (2001), The Ecohydrological role of soil texture in a water-limited ecosystem, *Water Resour. Res.*, *37*(12), 2863–2872, doi:10.1029/2000WR000121.

Ferré, T. P. A., A. Binley, J. Geller, E. Hill, and T. Illangasekare (2005), Hydrogeophysical methods at the laboratory scale, in *Hydrogeophysics*, edited by Y. Rubin and S. S. Hubbard, pp. 441–463, Springer, New York.

Friedman, S. P. (2005), Soil properties influencing apparent electrical conductivity: A review, *Comput. Electron. Agric.*, *46*, 45–70, doi:10.1016/j.compag.2004.11.001.

Gee, G., and D. Or (2002), Particle-size analysis, in *Methods of Soil Analysis. Part 4, Physical Methods, Soil Sci. Soc. Am. Book Ser.*, vol. 5, edited by J. H. Dane and G. C. Topp, pp. 255–293, Soil Sci. Soc. of Am., Madison, Wis.

Goovaerts, P. (1997), *Geostatistics for Natural Resources Evaluation*, 512 pp., Oxford Univ. Press, New York.

Goovaerts, P. (1999), Geostatistics in soil sciences: State-of-the-art and perspectives, *Geoderma*, *89*, 1–45, doi:10.1016/S0016-7061(98)00078-0.

Grant, L., M. Seyfried, and J. McNamara (2004), Spatial variation and temporal stability of soil water in a snow-dominated, mountain catchment, *Hydrol. Processes*, *18*(18), 3493–3511, doi:10.1002/hyp.5798.

Grauch, V. J. S., and P. S. Millegan (1998), Mapping intrabasinal faults from high-resolution aeromagnetic data, *Leading Edge*, *17*, 53–55, doi:10.1190/1.1437822.

Hendrickx, J. M. H., and R. G. Kachanoski (2002), Nonintrusive electromagnetic induction, in *Methods of Soil Analysis. Part 4 Physical Methods, Soil Sci. Soc. Am. Book Ser.*, vol. 5, edited by J. H. Dane and G. C. Topp, pp. 1297–1306, Soil Sci. Soc. of Am., Madison, Wis.

Huisman, J. A., S. S. Hubbard, J. D. Redman, and A. P. Annan (2003), Measuring soil water content with ground penetrating radar: A review, *Vadose Zone J.*, *2*, 476–491.

Hyndman, D., and J. Tronicke (2005), Hydrogeophysical case studies at the local scale: The saturated zone, in *Hydrogeophysics*, edited by Y. Rubin and S. S. Hubbard, pp. 391–412, Springer, New York.

Kachanoski, R. G., and E. de Jong (1988), Scale dependence and the temporal persistence of spatial patterns of soil water storage, *Water Resour. Res.*, *24*(1), 85–91, doi:10.1029/WR024i001p00085.

Lane, S., and J. H. Chandler (2003), Editorial: The generation of high quality topographic data for hydrology and geomorphology: New data sources, new applications and new problems, *Earth Surf. Processes Landforms*, *28*, 229–230, doi:10.1002/esp.479.

Lesch, S. M., D. J. Strauss, and J. D. Rhoades (1995a), Spatial prediction of soil salinity using electromagnetic induction techniques: 1. Statistical prediction models: A comparison of multiple linear regression and cokriging, *Water Resour. Res.*, *31*(2), 373–386, doi:10.1029/94WR02179.

Lesch, S. M., D. J. Strauss, and J. D. Rhoades (1995b), Spatial prediction of soil salinity using electromagnetic induction techniques: 2. An efficient spatial sampling algorithm suitable for multiple linear regression model identification and estimation, *Water Resour. Res.*, *31*(2), 387–398, doi:10.1029/94WR02180.

Lesch, S. M., J. D. Rhoades, and D. L. Corwin (2000), The ESAP-95 version 2.01R user manual and tutorial guide, *Res. Rep. 146*, George E. Brown, Jr., Salinity Lab., Agric. Resour. Serv., U. S. Dep. of Agric., Riverside, Calif.

Marks, D., K. R. Cooley, D. C. Robertson, and A. Winstral (2001), Long-term snow database, Reynolds Creek Experimental Watershed, Idaho, United States, *Water Resour. Res.*, *37*(11), 2835–2838, doi:10.1029/2001WR000416.

McDonnell, J. J., et al. (2007), Moving beyond heterogeneity and process complexity: A new vision for watershed hydrology, *Water Resour. Res.*, *43*, W07301, doi:10.1029/2006WR005467.

McNeill, J. D. (1980), Electromagnetic terrain conductivity measurement at low induction numbers, *Tech. Note TN-6*, Geonics, Ontario, Alberta, Canada. (Available at http://www.geonics.com/pdfs/technicalnotes/tn6.pdf)

Merz, B., and E. J. Plate (1997), An analysis of the effects of spatial variability of soil and soil moisture on runoff, *Water Resour. Res.*, *33*(12), 2909–2922, doi:10.1029/97WR02204.

Michaelides, K., and M. D. Wilson (2007), Uncertainty in predicted runoff due to patterns of spatially variable infiltration, *Water Resour. Res.*, *43*, W02415, doi:10.1029/2006WR005039.

Natural Resources Conservation Service (1999), *Soil Taxonomy: A Basic System of Soil Classification for Making and Interpreting Soil Surveys, Agric. Handb. 436*, 2nd ed., 869 pp., U. S. Dep. of Agric., Washington, D. C.

Newman, B. D., B. P. Wilcox, S. R. Archer, D. D. Breshears, C. N. Dahm, C. J. Duffy, N. G. McDowell, F. M. Phillips, B. R. Scanlon, and E. R. Vivoni (2006), Ecohydrology of water-limited environments: A scientific vision, *Water Resour. Res.*, *42*, W06302, doi:10.1029/2005WR004141.

Paul, C. R. (2004), *Electromagnetics for Engineers*, 403 pp., John Wiley, Hoboken, N. J.

Rhoades, J. D., F. Chanduvi, and S. M. Lesch (1999), Soil salinity assessment: Methods and interpretation of electrical conductivity measurements, *FAO Rep. 57*, 150 pp., Food and Agric. Organ., Rome.

Robinson, D. A., H. Abdu, S. B. Jones, M. Seyfried, I. Lebron, and R. Knight (2008a), Eco-geophysical imaging of watershed-scale soil patterns links with plant community spatial patterns, *Vadose Zone J.*, *7*, 1132–1138, doi:10.2136/vzj2008.0101.

Robinson, D. A., et al. (2008b), Advancing process-based watershed hydrological research using near-surface geophysics: A vision for, and review of, electrical and magnetic geophysical methods, *Hydrol. Processes*, *22*(18), 3604–3635, doi:10.1002/hyp.6963.

Robinson, D. A., C. S. Campbell, J. W. Hopmans, B. K. Hornbuckle, S. B. Jones, R. Knight, F. Ogden, J. Selker, and O. Wendroth (2008c), Soil moisture measurement for ecological and hydrological watershed scale observatories: A review, *Vadose Zone J.*, *7*, 358–389, doi:10.2136/vzj2007.0143.

Rubin, Y., and S. S. Hubbard (2005), *Hydrogeophysics*, 523 pp., Springer, New York.

Schaap, M. G. (1999), Rosetta: Pedotransfer function software, version 1.2, U. S. Salinity Lab., Agric. Resour. Serv., U. S. Dep. of Agric., Riverside, Calif. (Available at http://www.ars.usda.gov/Services/docs.htm?docid=8953)

Selker, J. S., L. Thévenaz, H. Huwald, A. Mallet, W. Luxemburg, N. van de Giesen, M. Stejskal, J. Zeman, M. Westhoff, and M. B. Parlange (2006), Distributed fiber-optic temperature sensing for hydrologic systems, *Water Resour. Res.*, *42*, W12202, doi:10.1029/2006WR005326.

Seyfried, M., R. Harris, D. Marks, and B. Jacob (2001), Geographic database, Reynolds Creek Experimental Watershed, Idaho, United States, *Water Resour. Res.*, *37*(11), 2825–2829, doi:10.1029/2001WR000414.

Sheets, K., and J. Hendrickx (1995), Noninvasive soil water content measurement using electromagnetic induction, *Water Resour. Res.*, *31*(10), 2401–2409, doi:10.1029/95WR01949.

Sherlock, M., and J. J. McDonnell (2003), A new tool for hillslope hydrologists: Spatially distributed measurements of groundwater and soil water using electromagnetic induction, *Hydrol. Processes*, *17*(10), 1965–1978, doi:10.1002/hyp.1221.

Sivakumar, B. (2004), Dominant processes concept in hydrology: Moving forward, *Hydrol. Processes*, *18*(12), 2349–2353, doi:10.1002/hyp.5606.

Slaughter, C. W., D. Marks, G. N. Flerchinger, S. S. Van Vactor, and M. Burgess (2001), Thirty-five years of research data collection at the Reynolds Creek Experimental Watershed, Idaho, United States, *Water Resour. Res.*, *37*(11), 2819–2823, doi:10.1029/2001WR000413.

Tarboton, D. G., R. L. Bras, and I. Rodriguez Iturbe (1991), On the extraction of channel networks from digital elevation data, *Hydrol. Processes*, *5*(1), 81–100, doi:10.1002/hyp.3360050107.

Triantafilis, J., and S. M. Lesch (2005), Mapping clay content variation using electromagnetic induction techniques, *Comput. Electron. Agric.*, *46*(1–3), 203–237, doi:10.1016/j.compag.2004.11.006.

Triantafilis, J. A., I. Huckel, and I. O. A. Odeh (2001), Comparison of statistical prediction methods for estimating field-scale clay content using different combinations of ancillary variable, *Soil Sci.*, *166*(6), 415–427, doi:10.1097/00010694-200106000-00007.

Webster, R., and M. Oliver (2001), *Geostatistics for Environmental Scientists*, 271 pp., John Wiley, New York.

Western, A. W., R. B. Grayson, G. Blöschl, G. R. Willgoose, and T. A. McMahon (1999), Observed spatial organization of soil moisture and its relation to terrain indices, *Water Resour. Res.*, *35*(3), 797–810, doi:10.1029/1998WR900065.

Woolhiser, D. A., R. E. Smith, and J.-V. Giraldez (1996), Effects of spatial variability of saturated hydraulic conductivity on Hortonian overland flow, *Water Resour. Res.*, *32*(3), 671–678, doi:10.1029/95WR03108.

H. Abdu, Department of Biological and Irrigation Engineering, Utah State University, Logan, UT 84322, USA. (hiruy.abdu@aggiemail.usu.edu)

S. B. Jones, Department of Plants, Soils and Climate, Utah State University, Logan, UT 84322, USA.

D. A. Robinson, Department of Food Production, University of the West Indies, St. Augustine, Trinidad and Tobago.

M. Seyfried, Northwest Watershed Research Center, ARS, USDA, 800 Park Boulevard, Plaza IV, Suite 105, Boise, ID 83712, USA.